Supplementary Information (SI) for EES Batteries.
This journal is © The Royal Society of Chemistry 2026

Supporting information

Synergistic Effect Between Carbon-Confined Bismuth Nanoparticles and K^+-Ether Co-Intercalation Enables High-Rate Potassium Storage at -50 °C

Jiawei Gu[a,§], Jiali Lin[a,§], Ling Huang[a,§], Miao Liu[a*], Zhefei Sun[b], Xing Chen[a], Jiaqi Zhang[a], Mingxuan Luo[a], Qiaobao Zhang[a,b], Li Zhang[a,c*]

[a]College of Chemistry and Chemical Engineering, State Key Laboratory of Physical Chemistry of Solid Surfaces, Xiamen 361005, Fujian, China.

E-mails: zhangli81@xmu.edu.cn, liumiao11@xmu.edu.cn

[b]College of Materials, Fujian Key Laboratory of Surface and Interface Engineering for High Performance Materials, Xiamen Key Laboratory of High Performance Metals and Materials, Xiamen University, Xiamen, 361005, Fujian, China.

[c]Tan Kah Kee Innovation Laboratory, Xiamen University, Collaborative Innovation Center of Chemistry for Energy Materials, Xiamen University, Xiamen 361005, Fujian, China.

KEYWORDS: Carbon-confined bismuth nanoparticles, K^+-ether-solvent co-intercalation, ultralow temperature electrochemistry, K-ion battery/hybrid capacitor, 1,2-Dimethoxyethane

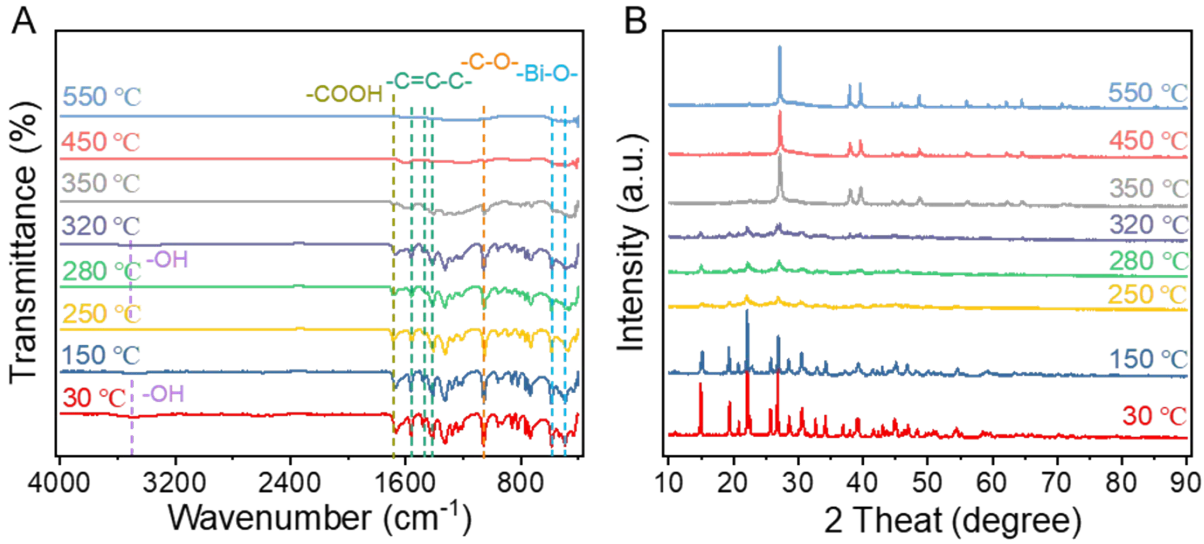

Figure S1. (A) FTIR spectra and (B) XRD patterns of bismuth subgallate hydrate at various annealing temperatures.

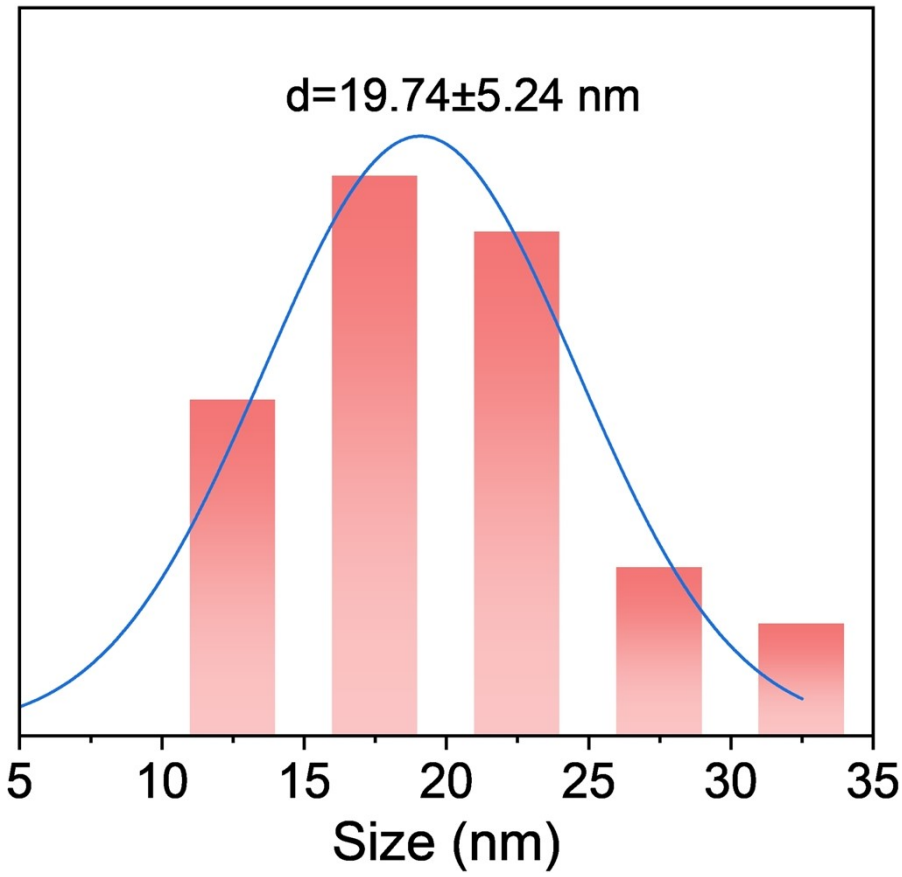

Figure S2. Particle size distribution of Bi nanoparticles in the Bi@CFs sample derived from TEM measurements.

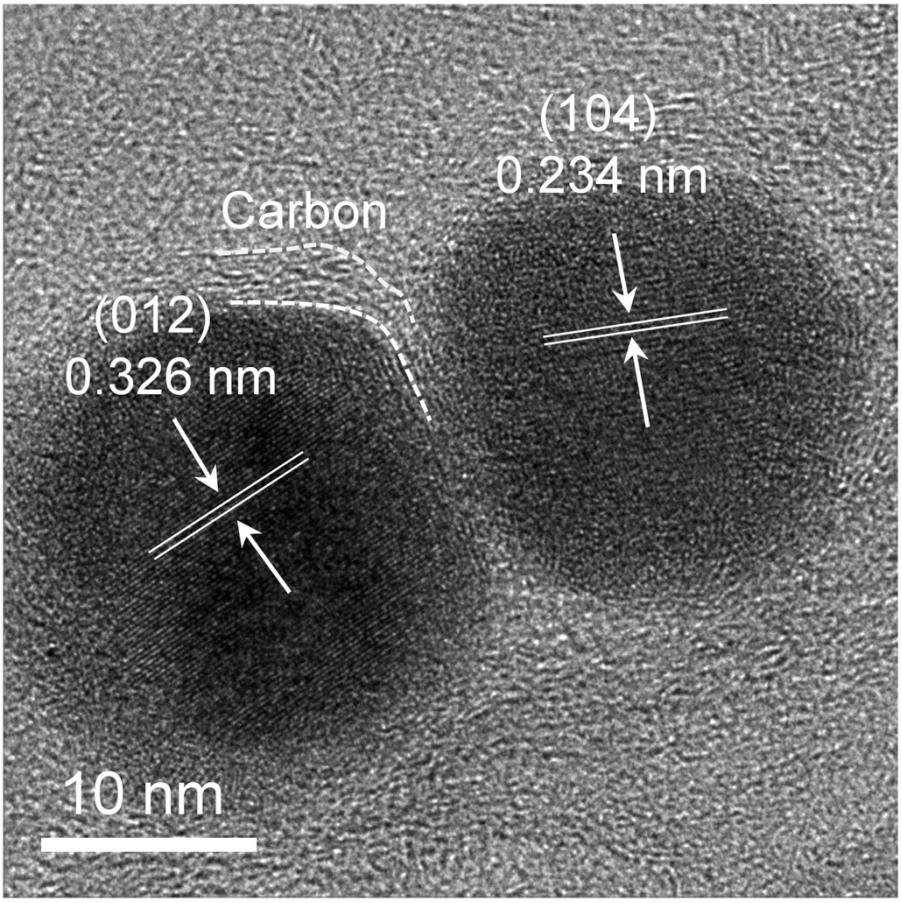

Figure S3. HRTEM image of the Bi@CFs sample.

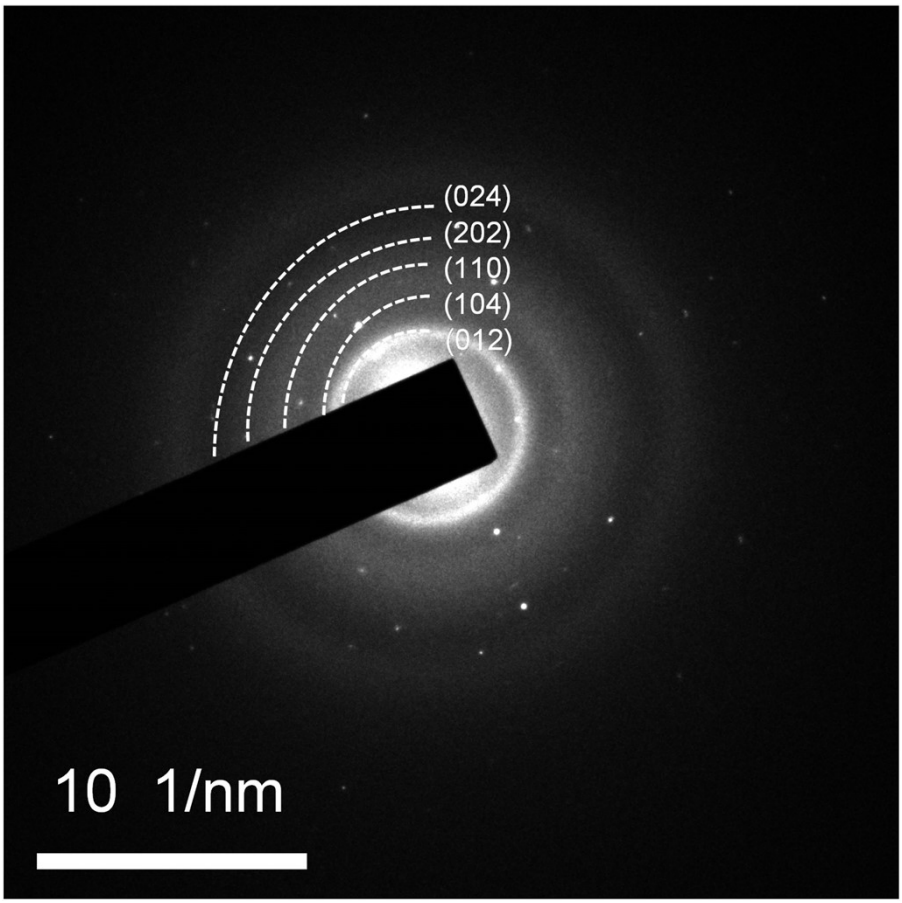

Figure S4. Selected area electron diffraction (SAED) pattern of the Bi@CFs sample.

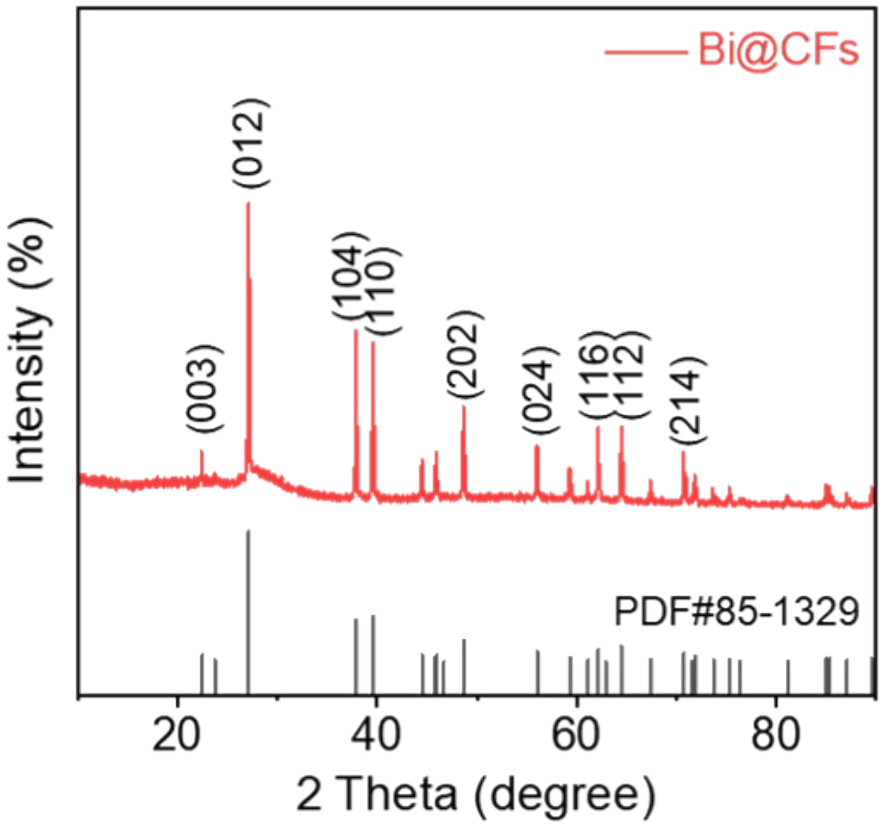

Figure S5. XRD pattern of the Bi@CFs sample.

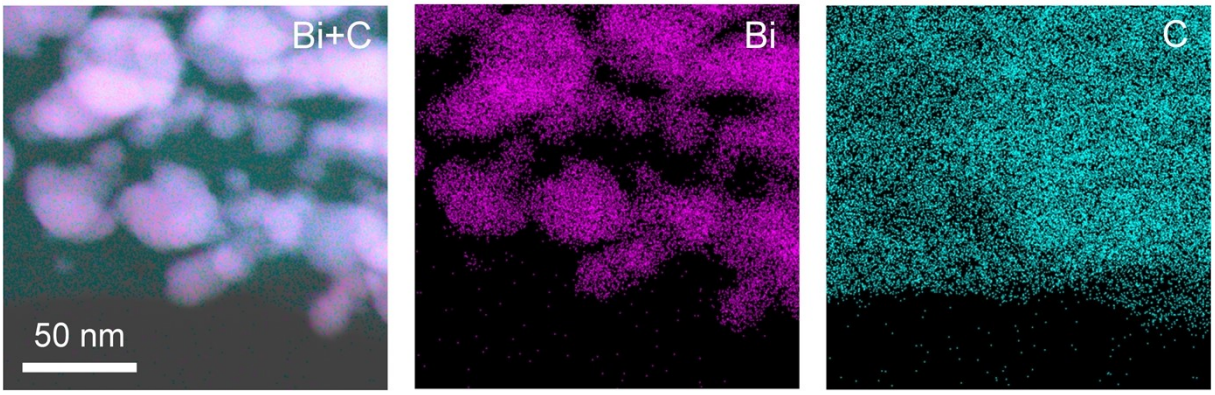

Figure S6. Element mapping of Bi and C in the Bi@CFs composite.

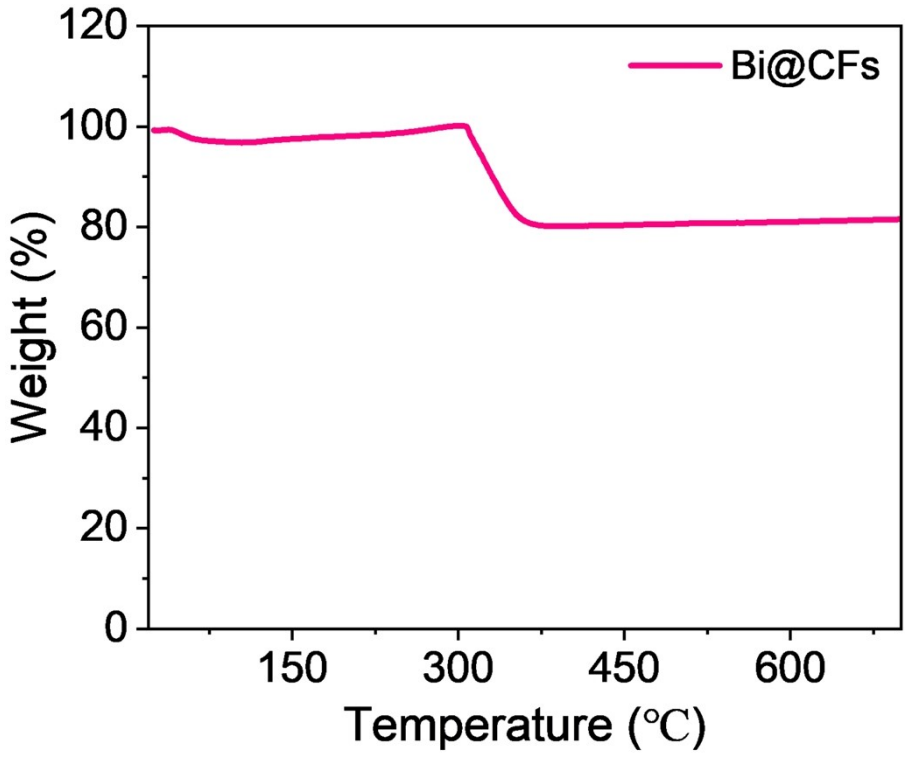

Figure S7. TGA curve of the basic bismuth subgallate hydrate.

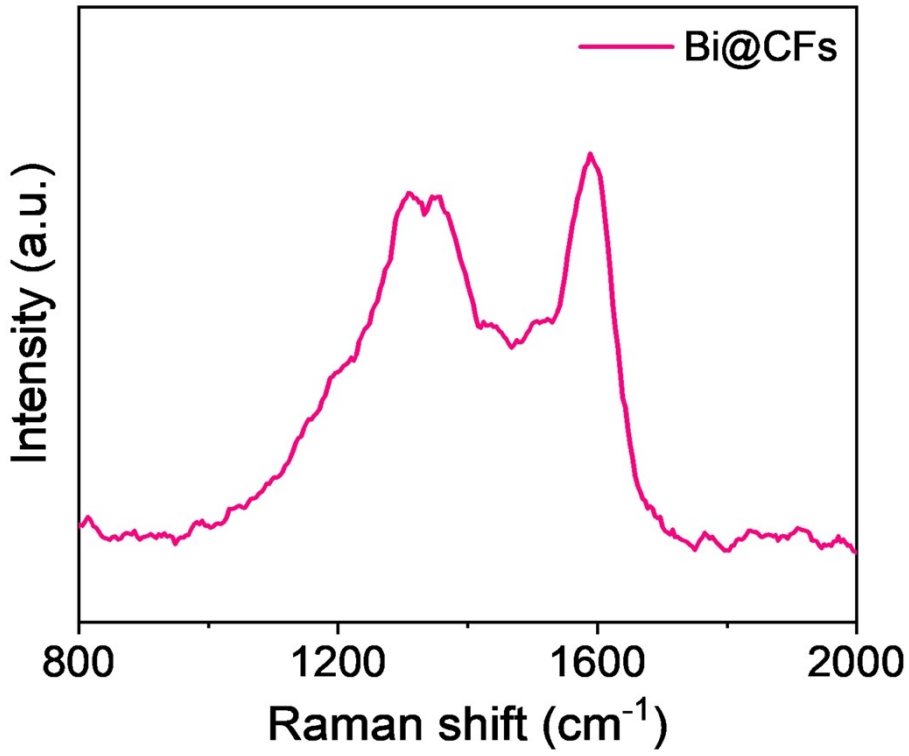

Figure S8. Raman spectrum of the Bi@CFs sample.

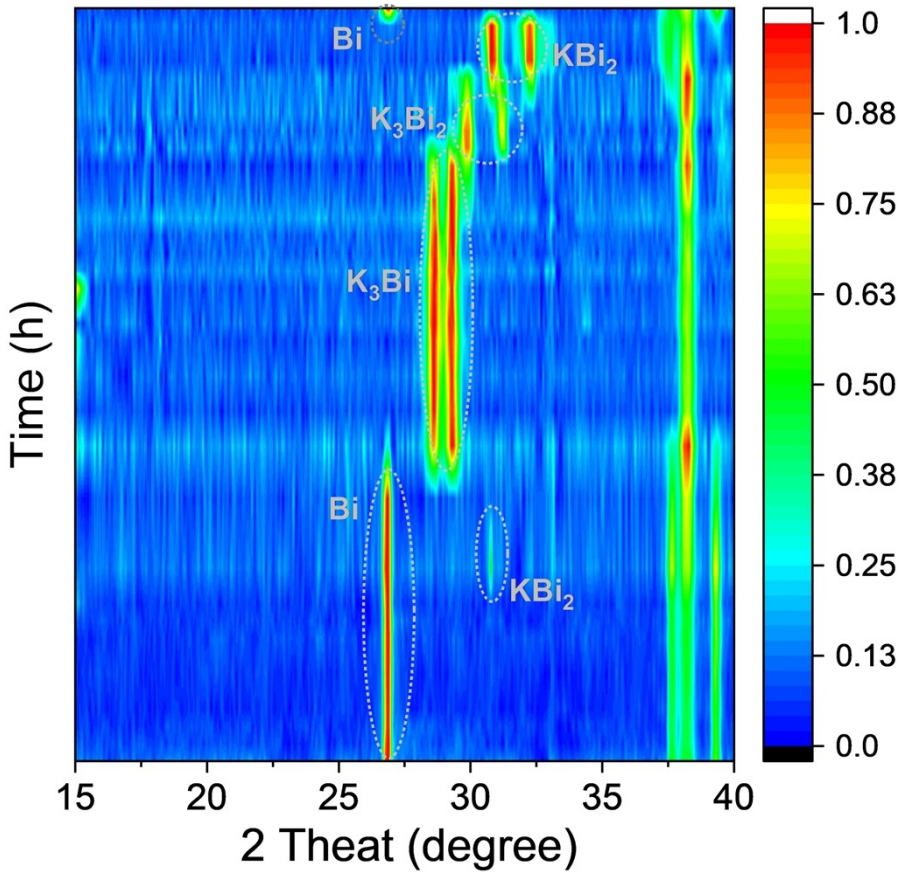

Figure S9. In situ XRD contour mapping of the Bi@CFs electrode during the first cycle.

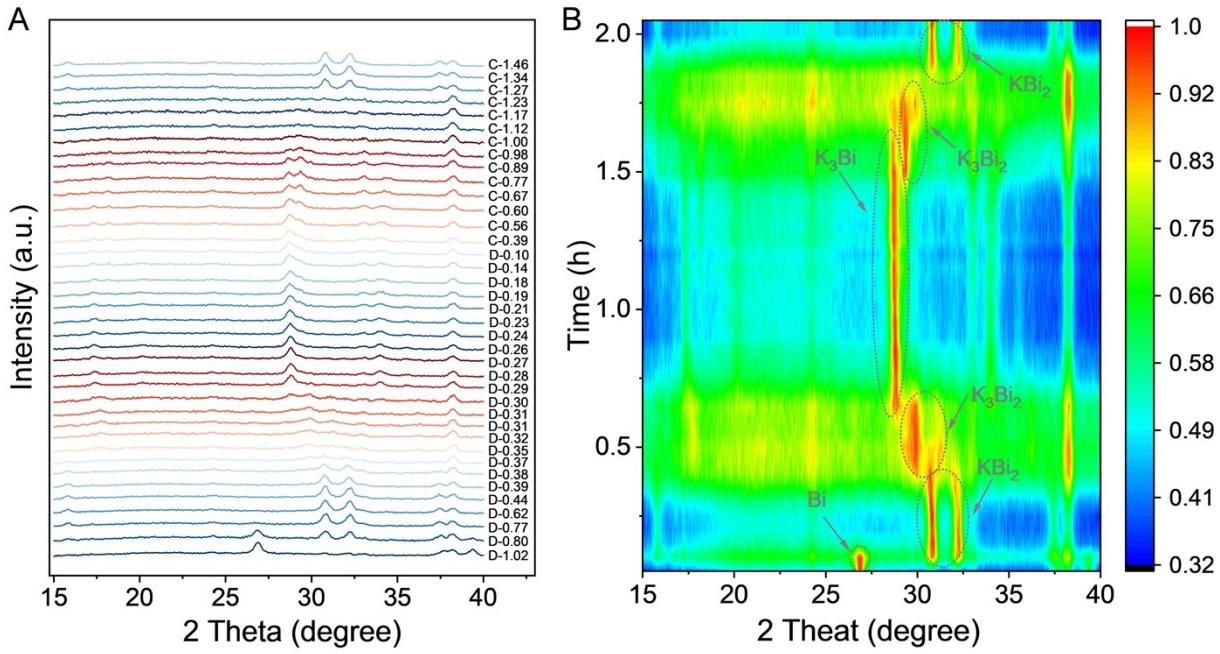

Figure S10. In situ XRD patterns of the Bi@CFs electrode during the second cycle: (A) corresponding diffraction profiles and (B) contour mapping.

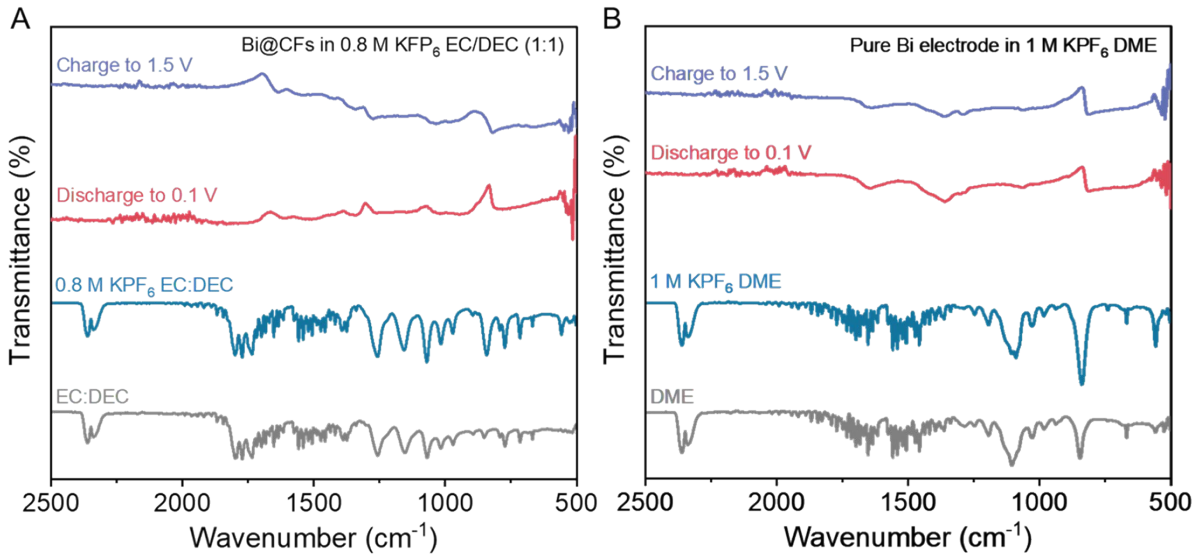

Figure S11. (A) Ex situ FTIR spectra of Bi@CFs electrode in the carbonate-based electrolyte discharge and charge stages. (B) Ex situ FTIR spectra of pure Bi electrode in the DME-based electrolyte discharge and charge stages.

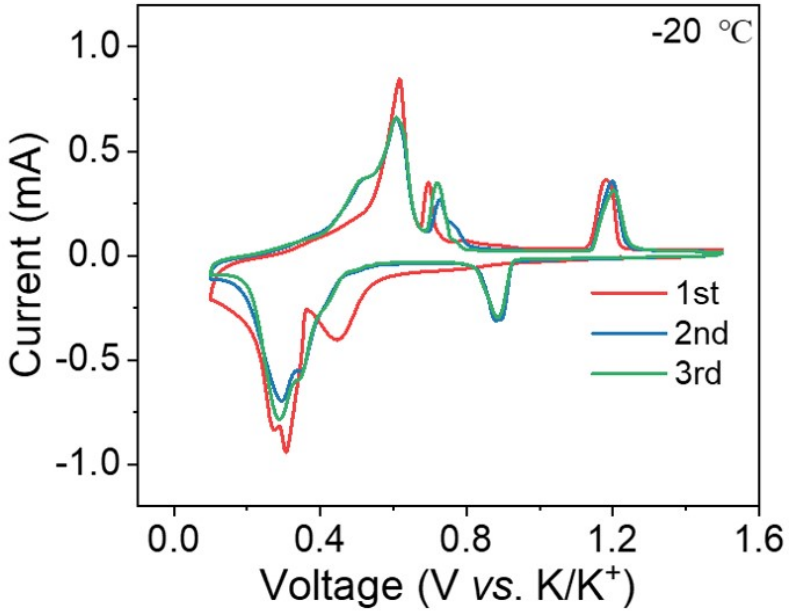

Figure S12. CV curves of the Bi@CFs electrode at a scan rate of 0.2 mV s^{-1} in the potential range of 0.1-1.5 V (-20 °C).

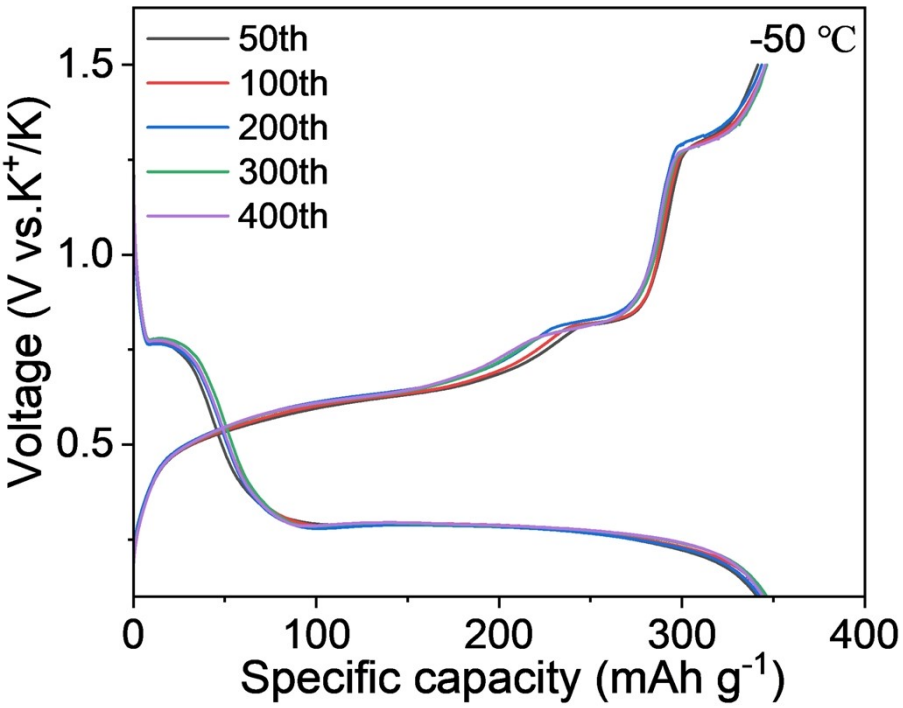

Figure S13. GCD profiles of the Bi@CFs electrode after various cycles under -50 °C.

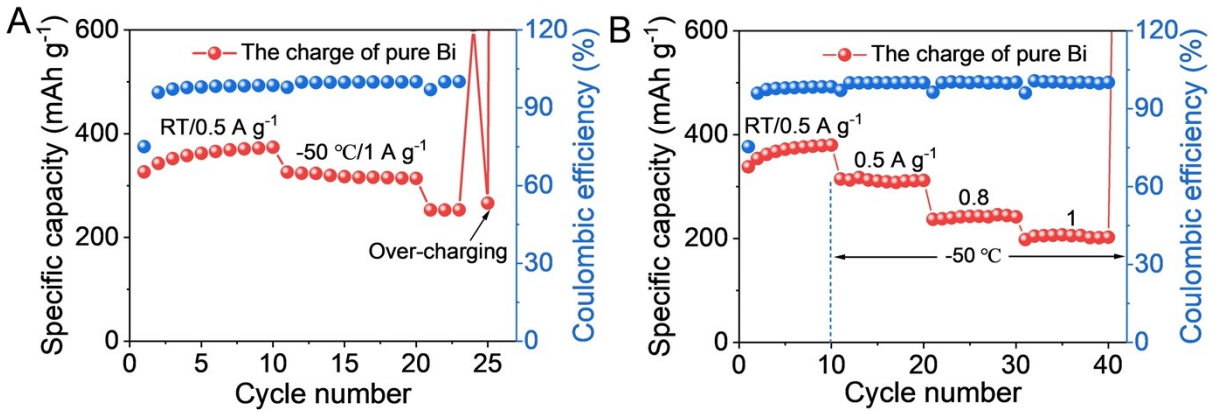

Figure S14. (A) Electrochemical cycling stability and (B) rate performance of the pure Bi electrode at -50 °C.

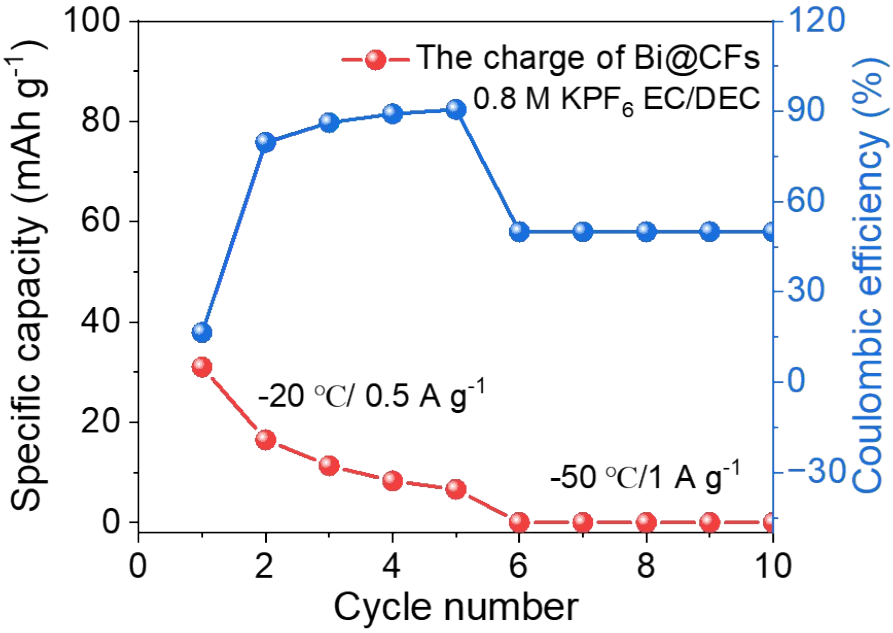

Figure S15. Electrochemical cycling stability of Bi@CFs electrode in carbonate-based electrolyte at -50 °C.

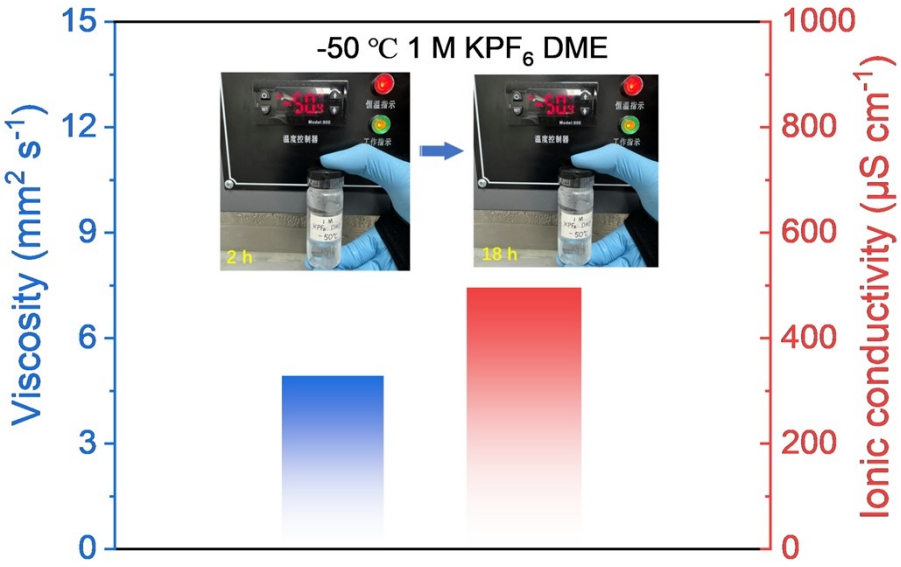

Figure S16. The viscosity and ionic conductivity of the DME-based electrolyte at -50 °C.

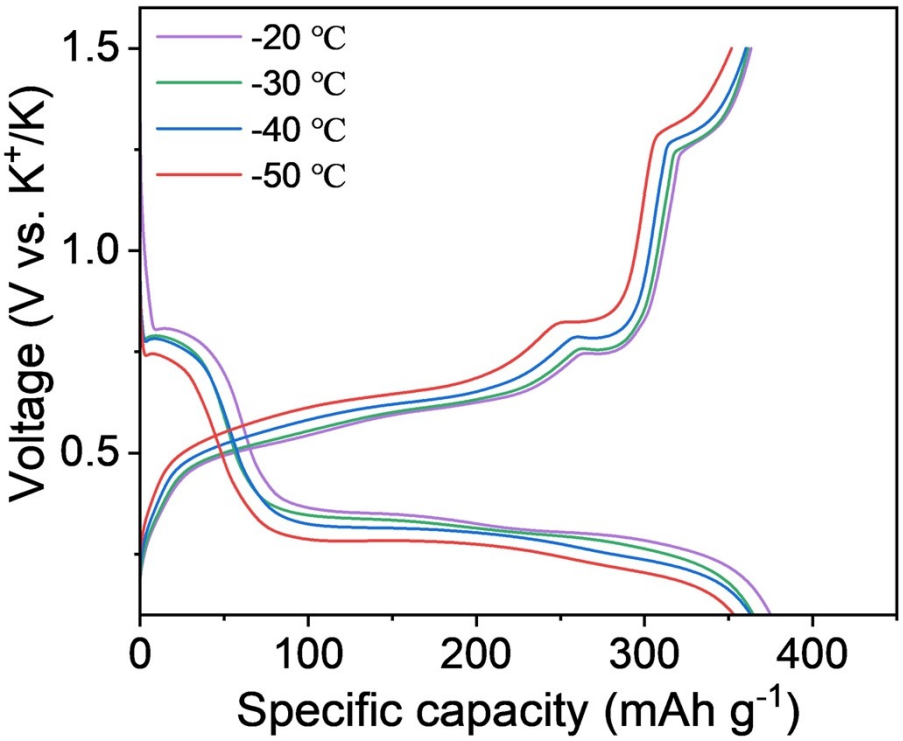

Figure S17. GCD profiles of the Bi@CFs electrode at 1 A g^{-1} under various temperatures.

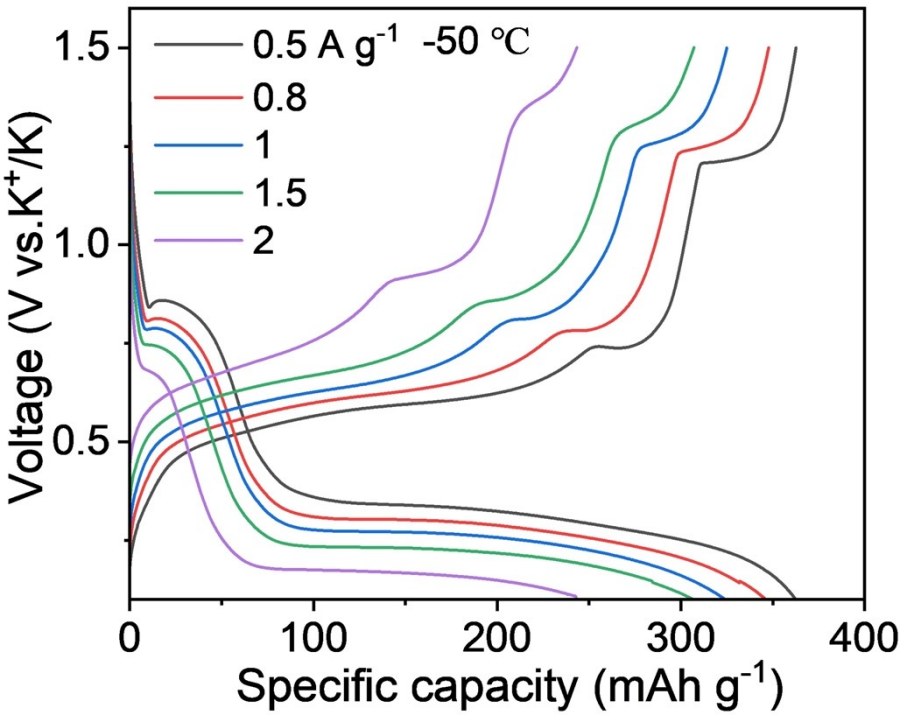

Figure S18. GCD profiles of Bi@CFs electrode at different current densities under -50 °C.

Table S1. The comparison of electrochemical performance between the Bi@CFs anode and previously reported anodes for SIBs and PIBs at various temperatures.[1-13]

Samples	Voltage range (V)	Capacity and Cycle stability (mAh g^{-1}/cycles)	Temperature (°C)	Refs.
Bi@CFs	**0.1~1.5**	**345.35@1 A g^{-1}/400**	**-50**	**This work**
Bi@C	0.01~1.5	246@0.1 A g^{-1}/10	-40	Carbon Energy. 2024, 6, e531.
HC	0.01~2	128@0.026 A g^{-1}/400	-40	Angew. Chem. Int. Ed. 2023, 62, e202307122.
CNTs	0.01~3.0	230.8@0.1 C/1 167.8@0.1 C/1 76.7@0.1 C/1	-20 -40 -50	Chem. Eng. J. 2022, 429, 132272.
NCG-EE-K	0.1~3	85@0.05 A g^{-1}/150	-40	Adv. Funct. Mater. 2023, 33, 2209775.
TiO_2-rGO	0.01~2.5	120@5 C/1500 100@5 C/1500	-20 -40	J. Alloys and Compd. 2020, 835, 155413.
$Na_2Ti_6O_{13}$@C	0.1~2	25@0.1 C/6	-40	Batteries & Supercaps. 2023, 6, e202200549.
$NaV_{1.25}Ti_{0.75}O_4$	0.01~2.3	95@0.02 A g^{-1}/2	-20	Adv. Energy Mater. 2018, 8, 1801162.
NPT/C-CNTs	1.5~3.0	113@0.5 C/1	-20	RSC Adv. 2016, 6, 70277.
KPTCDA	0~2	17@0.0558 A g^{-1}/1	-20	Angew. Chem. Int. Ed. 2024, 63, e202315624.
$NaTi_2(PO_4)_3$@C	1.5~3	102.35@0.2C/200	-20	J. Power Sources. 2020, 477, 228735.
Bi@3DCF	0~1.5	200@1 A g^{-1}/500	-20	Mater. Today Energy. 2021, 20, 100627.
$FeSe_2$/rGO	0.5~3.0	216.7@1 A g^{-1}/200	-40	Chem. Eng. J. 2021, 422, 130054.
Graphite	0~2.5	73@0.1 A g^{-1}/25	-40	Angew. Chem. Int. Ed. 2021, 60, 23858-23862.

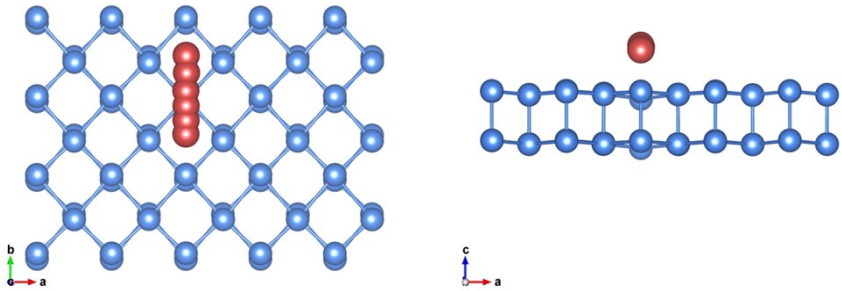

Figure S19. The diagrams of migration path on the surface of pure Bi electrode.

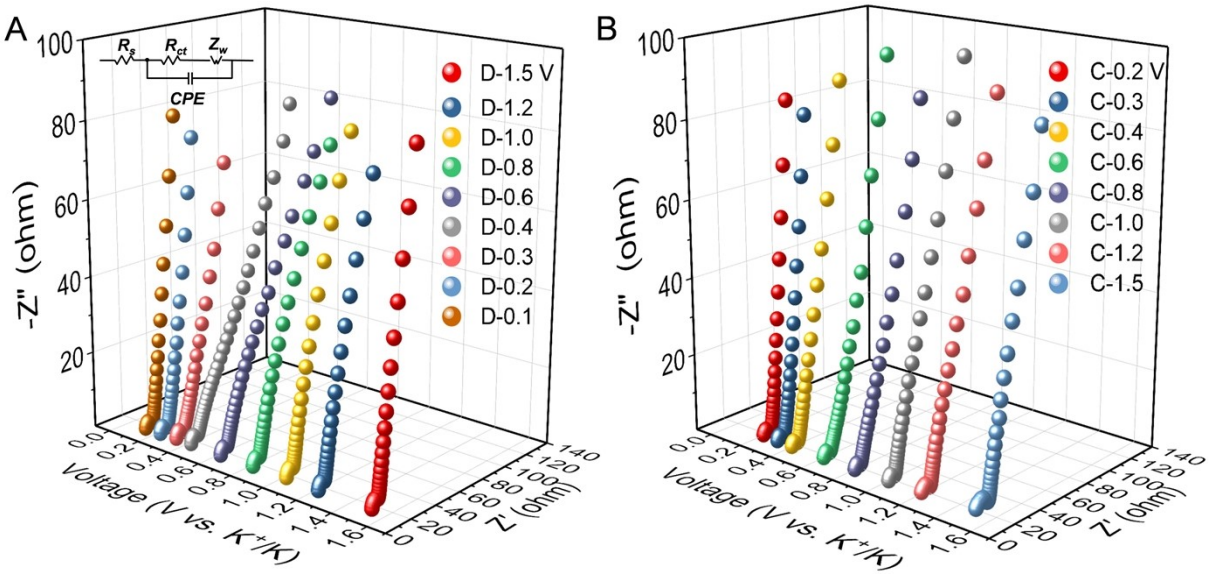

Figure S20. In situ EIS measurements of the Bi@CFs electrode during (A) discharge and (B) charge processes at 0.3 A g^{-1} under -50 °C.

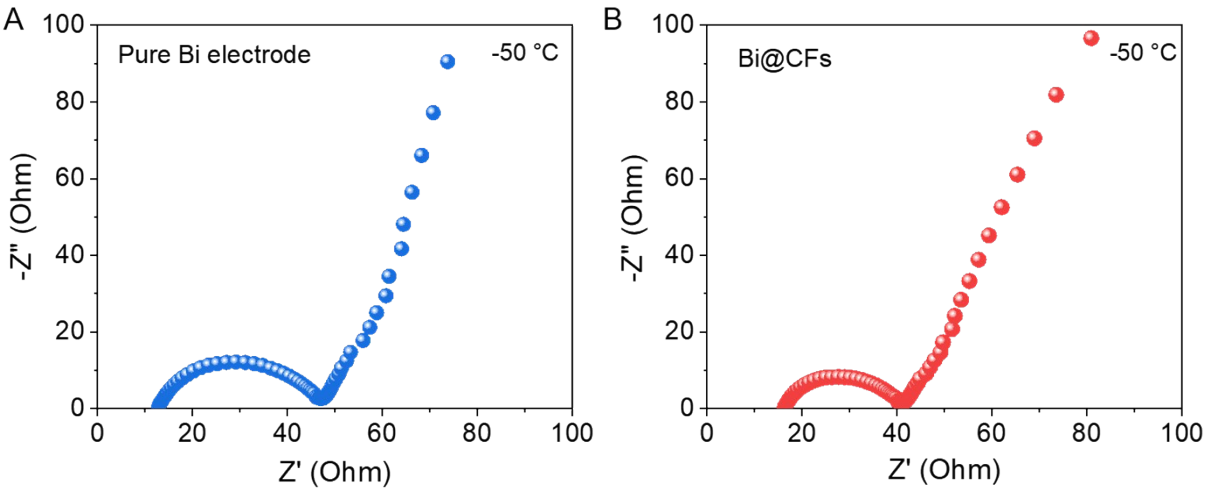

Figure S21. Ex-suit EIS measurements of (A) the pure Bi and (B) Bi@CFs electrodes after five cycles.

Table S2. Comparison of charge transfer impedance values between this work and previously reported literature under low-temperatures.[14-17]

Samples	Cycles	R_{ct} (Ω)	Temperature (°C)	Ref.
LBL-modified graphite	Initial	66.7	-20	ACS Appl. Energy Mater. 2023, 6, 12371-12378
Mo,S-LTO/Mx	Initial	> 500	-20	Mater. Today Chem. 2022, 26, 101145
SH1600	Initial	167.5	-20	J. Energy Storage. 2024, 102, 114056
Gen 2 BN/FEC BN/EC+FEC	After 3 cycles	130.5 97.67 101.3	-20	ACS Appl. Mater. Interfaces. 2022, 14, 11910-11918
Bi@CFs	**After 2 cycles**	**< 30**	**-50**	**This work**

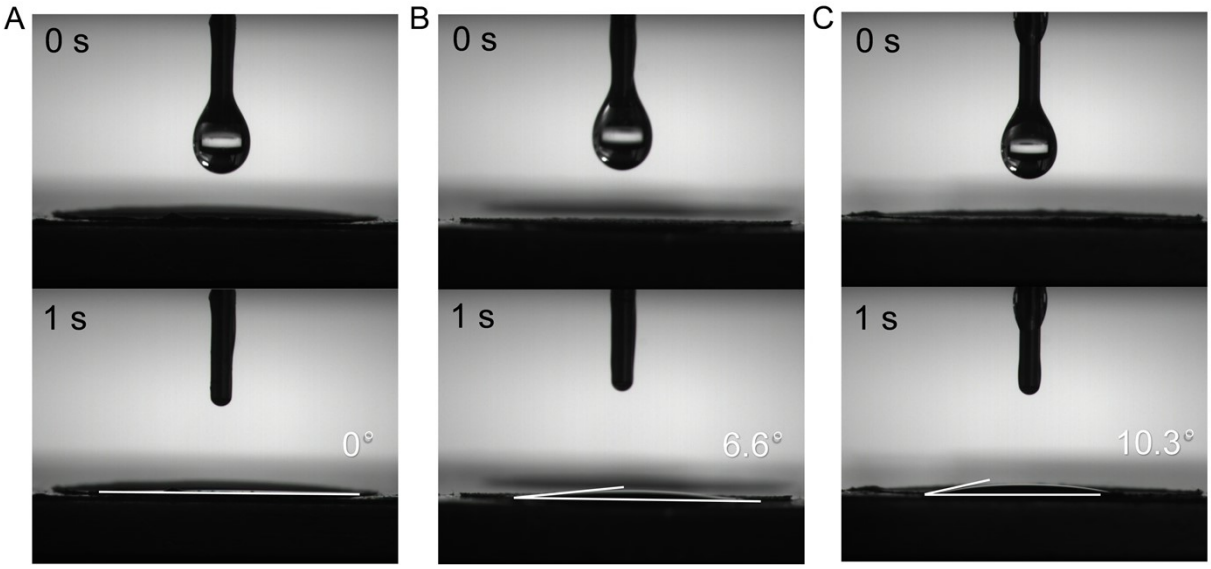

Figure S22. The contact angles of DME-based electrolyte on (A) Bi@CFs electrode and (B) pure Bi electrode. (C) Contact angles of EC/DEC-based electrolyte on the Bi@CFs electrode.

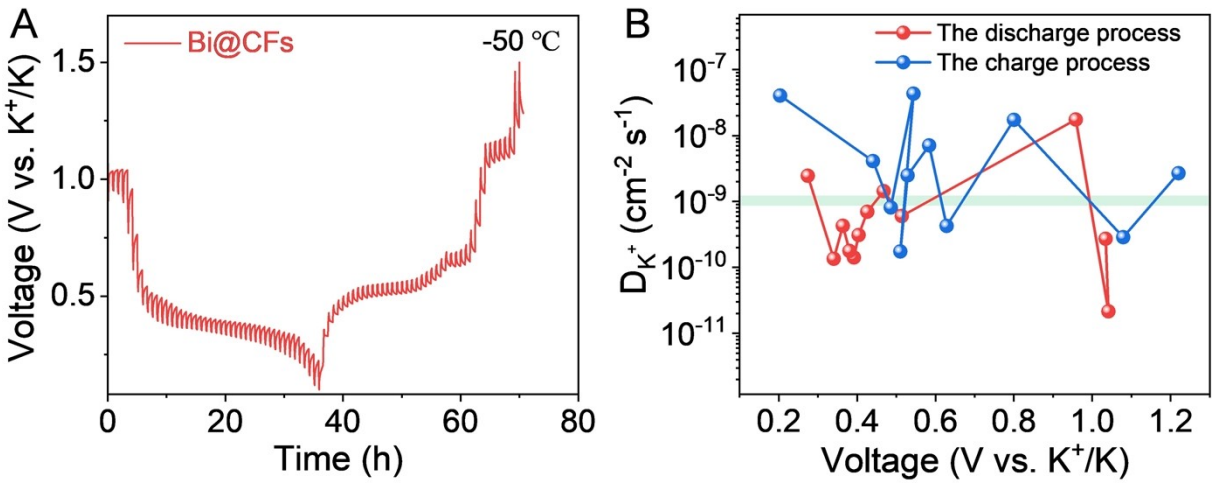

Figure S23. (A) Galvanostatic intermittent titration (GITT) profile of the Bi@CFs electrode at 50 mA g^{-1} under -50 °C, and (B) corresponding calculation of the K-ion diffusion coefficient.

The value of D_{k^+} was calculated using the simplified Fick's second law, as represented by equation (5):[18]

$$D = \frac{4}{\pi\tau}\left(\frac{m_B V_M}{M_B A}\right)^2\left(\frac{\Delta E_s}{\Delta E_\tau}\right)^2 \quad (1)$$

Where τ is the pulse duration, m_B, M_B, and V_M correspond to the mass, molar mass, and molar volume of electrode, A is difined as the interfacial area between electrode and electrolyte.[19]

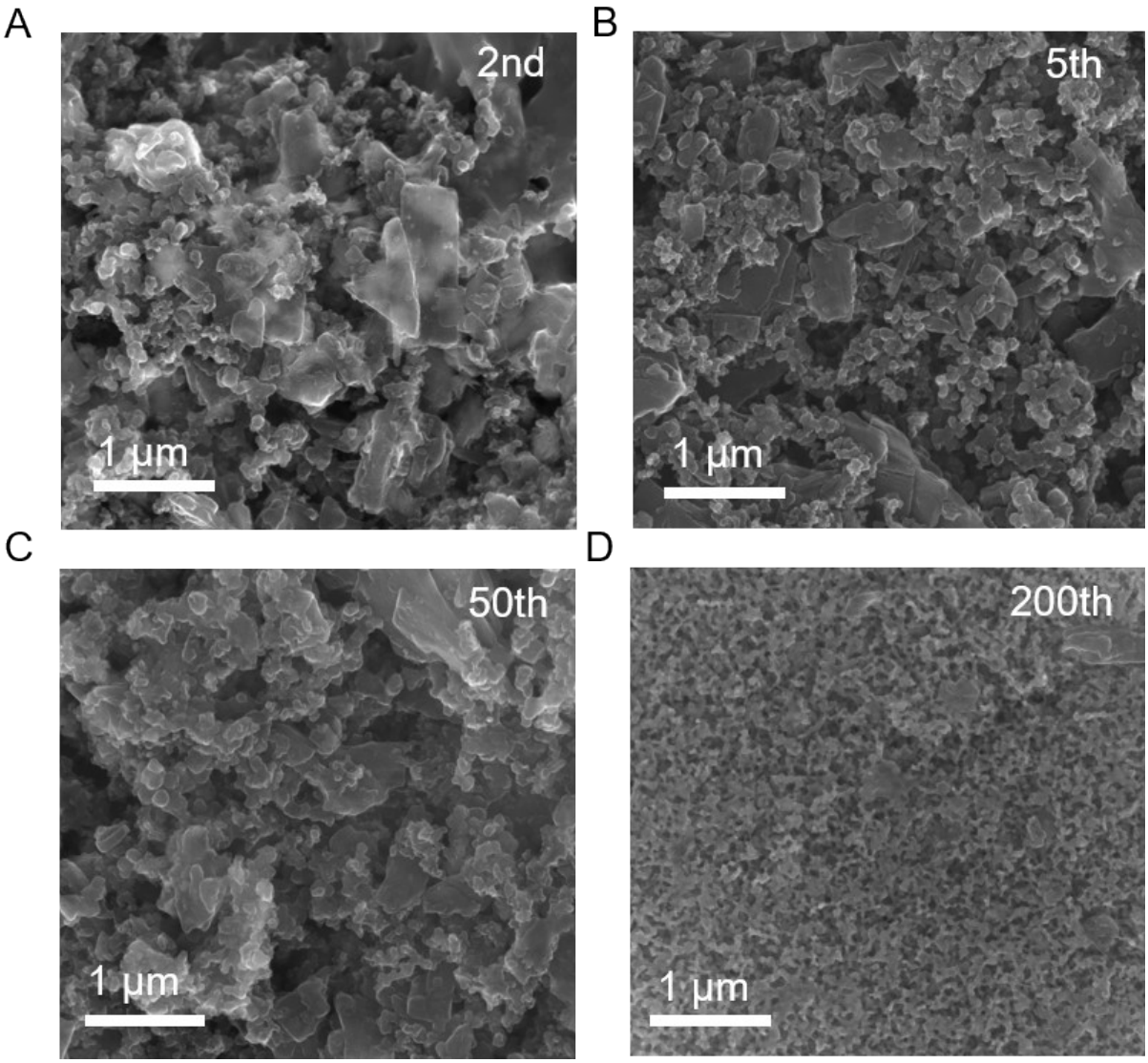

Figure S24. SEM images of the Bi@CFs electrodes after (A) 2nd, (B) 5th, (C) 50th and (D) 200th cycles.

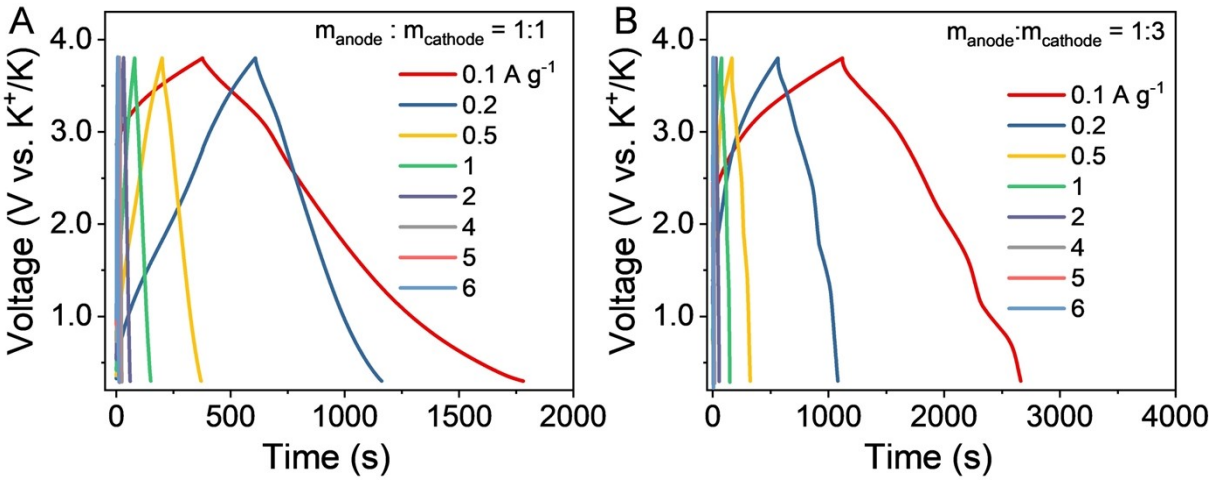

Figure S25. GCD profiles of the Bi@CFs/AC hybrid capacitors with various anode-to-cathode mass ratios: (A) 1:1 and (B) 1:3.

REFERENCES

1. L. Liu, S. Li, L. Hu, X. Liang, W. Yang, X. Yang, K. Hu, C. Hou, Y. Han and S. Chou, *Carbon Energy*, 2024, **6**, e531.
2. J. Chen, D. An, S. Wang, H. Wang, Y. Wang, Q. Zhu, D. Yu, M. Tang, L. Guo and H. Wang, *Angew. Chem. Int. Ed.*, 2023, **62**, e202307122.
3. D. Wang, J. Zhang, X. Li, L. Liu, M. Yuan, B. Cao, A. Li, X. Chen, R. Yang and H. Song, *Chem. Eng. J.*, 2022, **429**, 132272.
4. K. Lee, M. J. Lee, J. Lim, K. Ryu, M. Li, S. Noda, S. J. Kwon and S. W. Lee, *Adv. Funct. Mater.*, 2022, **33**, 2209775.
5. D.-R. Deng, X.-Y. Cui, Q.-H. Wu, M.-S. Zheng and Q.-F. Dong, *J. Alloys and Compd.*, 2020, **835**, 155413.
6. Q. S. Lai, J. J. Mu, Z. M. Liu, L. K. Zhao, X. W. Gao, D. R. Yang, H. Chen and W. B. Luo, *Batteries & Supercaps*, 2023, **6**, e202200549.
7. Q. Li, K. Jiang, X. Li, Y. Qiao, X. Zhang, P. He, S. Guo and H. Zhou, *Adv. Energy Mater.*, 2018, **8**, 1801162.
8. L. Wang, B. Wang, G. Liu, T. Liu, T. Gao and D. Wang, *RSC Adv.*, 2016, **6**, 70277-70283.
9. L. Cheng, H. Lan, Y. Gao, S. Dong, Y. Wang, M. Tang, X. Sun, W. Huang and H. Wang, *Angew. Chem. Int. Ed.*, 2024, **63**, e202315624.
10. X. Zhang, M. Zeng, Y. She, X. Lin, D. Yang, Y. Qin and X. Rui, *J. Power Sources*, 2020, **477**, 228735.
11. B. Wang, H. Yang, Y. Feng, S. Zeng, L. Tan, R. Xu, L. Wang, R. Hu and Y. Yu, *Mater. Today Energy*, 2021, **20**, 100627.
12. Y. Tian, J. Lu, H. Tang, X. Wang, L. Zhang, P. Hu, L. Zhou, Y. Wang, Y. Guo, R. Khatoon, Q. Zhang, Q. He, Y. He, M. Qiu, Y. Hou and Z. Ye, *Chem. Eng. J.*, 2021, **422**, 130054.
13. J. Chen, Y. Peng, Y. Yin, Z. Fang, Y. Cao, Y. Wang, X. Dong and Y. Xia, *Angew. Chem. Int. Ed.*, 2021, **60**, 23858-23862.
14. Y. Yu, M. I. Levine, Z. Yang, S. Jeon, E. A. Stach and J. Xie, *ACS Appl. Energy Mater.*, 2023, **6**, 12371-12378.
15. Z. Pu, H. Li, Z. Yang, Y. Zhang, Y. Liu, G. Dong and Y. Li, *Mater. Today Chem*, 2022, **26**, 101145.
16. B. Lu, J.-X. Song, D.-R. Deng, G.-F. Li, Y. Zeng, S.-L. Cai, J.-C. Weng, X.-H. Fan, Y. Li and Q.-H. Wu, *J. Energy Storage*, 2024, **102**, 114056.
17. D.-J. Yoo, Q. Liu, O. Cohen, M. Kim, K. A. Persson and Z. Zhang, *ACS Appl. Mater. Interfaces*, 2022, **14**, 11910-11918.
18. J. Zhu, J. Fan, T. Cheng, M. Cao, Z. Sun, R. Zhou, L. Huang, D. Wang, Y. Li and Y. Wu, *Nano Energy*, 2020, **75**, 104939.
19. S. Trano, D. Versaci, M. Castellino, M. Fontana, L. Fagiolari, C. Francia and F. Bella, *Energy Mater.*, 2024, **4**, 400008.